JNeurosci
THE JOURNAL OF NEUROSCIENCE

Research Articles | Systems/Circuits

Ventromedial hypothalamic output to the anterior hypothalamic area evokes complex escape behavior

https://doi.org/10.1523/JNEUROSCI.0232-26.2026

Received: 5 February 2026
Revised: 24 October 2026
Accepted: 4 November 2026

Copyright © 2026 the authors

This Early Release article has been peer reviewed and accepted, but has not been through the composition and copyediting processes.The final version may differ slightly in style or formatting and will contain links to any extended data.

Alerts: Sign up at www.jneurosci.org/alerts to receive customized email alerts when the fully formatted version of this article is published.

Ventromedial hypothalamic output to the anterior hypothalamic area evokes complex escape behavior

Cailey M. Coletta[1], Arma'Rosa W. Mohead[1], Emily Krieger[1], Cody Porter[1], James A. Stewart[1], Brenton T. Laing[1, 2]

[1]Department of BioMolecular Sciences, University of Mississippi, Oxford, MS 38677, U.S.A.

[2]Interbeat Industries, Taylor, MS, 38673, U.S.A.

Correspondence should be addressed to Brenton Laing (btlaing@olemiss.edu)

Abstract

The ventromedial hypothalamus (VMH) and anterior hypothalamic area (AHA) contribute to the orchestration of defensive responses to threat. We set out to test the effects of VMH to AHA (VMH→AHA) stimulation on behavior, organ-systems physiology, circulating pro-inflammatory cytokine levels, and brain activity patterns that support escape behavior. We used optogenetics in male and female SF1-Cre mice for behavioral assays, physiological measurements, and brain activity pattern mapping. For the first time, we demonstrate that VMH^{SF1}→AHA photostimulation increases complex escape behavior that requires three-dimensional navigation. Even in anesthetized mice, VMH→AHA photostimulation increases fractional shortening of the heart consistent with sympathetic arousal. In addition, we demonstrate that VMH→AHA photostimulation increases levels of the pro-inflammatory cytokine IL-6. In the brain, we find significant elevations of activity in the lateral habenula, anterior hypothalamic area, ventral premammillary nucleus, ventrolateral periaqueductal gray, and locus coeruleus.

Significance statement: We demonstrate that VMH→AHA photostimulation increases escape behavior that depends on a three dimensional route of navigation, increases levels of the cytokine IL-6, as well as increases activity in the lateral habenula, ventral premammillary nucleus, ventrolateral periaqueductal gray, and locus coeruleus. This work informs how hypothalamic circuitry drives behavioral and physiological responses that facilitate escape from threats in the environment.

JNeurosci Accepted Manuscript

1. Introduction

Walter B. Cannon's work on fight or flight (Cannon, 1953) has served as a framework for the conceptualization of coordination between threat perception, physiology, and behavior. Mice conduct risk assessment during exposure to threatening stimuli (Blanchard et al., 2001), which facilitates an adaptive response within the state space of all potential responses. Simple defensive behaviors such as darting and freezing can be difficult to distinguish from exploration and immobile behaviors. However, complex escape behaviors depend on three-dimensional environmental navigation that includes opportunity assessment and execution of a motor plan(Wang et al., 2021a). Mice spontaneously explore escape routes with preference for routes that have the highest survival probability, minimal path distance, and optimal angle relative to the shelter(Claudi et al., 2022). In the presence of threat, the motivation to explore escape routes can be elevated.

Many neuronal circuits are involved in the planning and execution of three-dimensional exploration under threat conditions. The ventromedial hypothalamus (VMH) and anterior hypothalamic area (AHA) are both associated with the organization of responses to threats in the environment (Wang et al., 2015; Laing et al., 2025). VMH activity patterns represent predator identity and multiple predator-evoked defensive states such as fear/anxiety, arousal, neophobia, predator imminence, and safety (Cheung et al., 2025). VMH soma activity becomes modulated during innate and conditioned threat exposure, contributes to multiple defensive actions that are context-dependent, and instantiates emotional states (Kunwar et al., 2015). AHA activity increases during threat exposure(Cezario et al., 2008) and sends efferent projections to the dorsal premammillary nucleus (PMd) as part of the hypothalamic defense network(Saper et al., 1978). Further, it is known that VMH to AHA (VMH^{SF1}→AHA) projections decrease immobility in an open arena, and that VMH^{SF1} photostimulation increases sympathetic output to the heart (Wang et al., 2015).

Despite extensive testing of these individual responses to threat, the extent to which defensive responses can be evoked by VMH^{SF1}→AHA projection activation has not been evaluated in an ethologically relevant context. Further, little is known about how behavioral states correspond to organ-systems physiology and circulating factors. In the present study, we tested the effect of VMH^{SF1}→AHA stimulation on complex escape behavior and indicators of peripheral autonomic arousal consistent with flight responses. To our knowledge, this is the first report of complex escape behavior evoked by VMH^{SF1}→AHA stimulation.

2. Methods

Neurosci Accepted Manuscript

2.1 Animals

All experimental procedures were conducted in accordance with the U.S. National Institutes of Health Guidelines for the Care and Use of Laboratory Animals and with the approval of the University of Mississippi Institutional Animal Care and Use Committee protocol 24-006. Heterozygous male and female SF1-Cre(Dhillon et al., 2006) (Tg(NR5a1-cre)7Lowl/J; IMSR Cat # JAX:012462; The Jackson Laboratory, ME, USA) were used along with their Cre-negative littermates as controls. Thus, experimenters did not assign a balanced number of mice for males and females to each group since this was determined by the proportion of offspring in each group. This line is validated for selective targeting of the ventromedial hypothalamus(Bingham et al., 2006). Prior to surgery, mice were group-housed (up to 5 per cage) in temperature and humidity-controlled rooms on a 12-h light/dark cycle. Mice had ad libitum access to water and rodent chow (Teklad Global 18% Protein Rodent Diet, Teklad Diets, Madison, WI).

2.2 Stereotaxic viral injections

Stereotaxic microinjection was conducted using a stereotaxic apparatus (David Kopf Instruments, CA, USA) and a micromanipulator (Narishige, NY, USA) with custom-pulled pipettes (20-30 µm). Mice were administered post-operative meloxicam (5 mg/kg) for analgesia. All injections were targeted at the VMH (AP: -1.6, ML: -0.2, DV: -5.6) and 200 µm fiber optics were implanted dorsal to the AHA on the right side of the brain (AP: -0.80, ML: +0.4, DV: -4.8). The virus used was AAV9-EF1a-FLEX-hChR2(H134R)-mCherry-WPRE-HGHpA. 50 nL of virus was injected into each mouse. All mice were monitored post-operatively to ensure full recovery, and experiments were not started until 2 weeks after the operation.

2.3 Optogenetic stimulation control

Doric Neuroscience Studio software v6.6.3 (Doric Lenses, Inc., Quebec City, Canada) was used to deliver square-wave pulses (10 ms, 20 Hz) that were gated by ANY-maze TTL signals. A PM100D (Thorlabs, Newton, NJ, USA) power-meter verified the intensity of the light at the tip of a fiber optic was between 10-15 mW. Animals were acclimated to experimental rooms for at least 1 hour prior to each experiment. Immediately before testing, mice were tethered to a 450 nm laser (Doric Lenses, Inc.) via fiber optic patch cables. Video acquisition was conducted with ANY-maze USB 2 cameras with varifocal lenses using ANY-maze software v7. ANY-maze was used to produce tracking, freezing, and locomotor data. Videos were manually timestamped and scored using BORIS for jumping behavior.

2.4 Open Field Test

JNeurosci Accepted Manuscript

We tested the effects of photoactivation of VMH→AHA projections on locomotor behavior using the Open Field Test (OFT). We conducted the test in empty clear-walled arenas (30 cm x 30 cm) that had a thin layer of bedding on the floor. Arenas were housed inside of ENV-018V isolation chambers (Med Associates Inc., St. Albans, VT). The four-stage 12-minute testing session consisted of alternating 3-minute epochs. During the first and third epoch, the laser was off. During the second and fourth epoch, the laser was on.

2.5 Complex Escape Task

Immediately following the Open Field Test, a 45° wire-grid ramp that was attached to a 3D-printed frame was inserted into one corner of the chamber. The four-stage complex escape task again utilized alternating 3-minute epochs. During the first and third epoch, the laser was off. During the second and fourth epoch, the laser was on. As soon as a mouse successfully mounted the top edge of the wall, that test was ended and the escape was considered a success. Latency to escape was calculated as the time from the laser-ON period to the moment of escape. For mice that did not escape the apparatus, the full 180 s was recorded.

2.6 Elevated Plus Maze

Within a week of the open field test, mice were tethered to the patch cord and returned to the open field box for 6 minutes. For the first 3 minutes, no laser stimulation was delivered. For the next 3 minutes, laser stimulation was delivered. This protocol was required because in our unpublished data from another cohort of VMH→AHA stimulation, the mice would evacuate the plus maze. Thus, once the stimulation was complete, mice were detached and then transferred to the elevated plus maze for a 5-minute recording. The standard elevated plus maze consisted of two open arms (30 x 5 cm) and two closed arms (30 x 5 cm) extending from a central platform (5 x 5 cm). The apparatus was elevated 40 cm from the floor. The room was illuminated to 300 lx via overhead lighting. Mice were placed onto the center platform and allowed to freely explore until the end of the session.

2.7 Echocardiograms

Echocardiographic assessments were performed using the VEVO 3100 Imaging System (FUJIFILM VisualSonics, Toronto, ON, Canada) as previously described(Lindsey et al., 2018; Qrareya et al., 2022). Mice were anesthetized with ~1% isoflurane delivered via nose cone and positioned supine on a heated imaging stage equipped with ECG electrodes for continuous monitoring of heart rate and respiration. Body temperature was assessed throughout the procedure using a rectal thermal probe, and maximal temperature values were recorded for each

J Neurosci Accepted Manuscript

imaging period. Prewarmed ultrasound gel was applied to the thoracic region after hair removal to optimize acoustic coupling.

The experimental design consisted of two sequential imaging periods: (1) a 180-second baseline acquisition with the laser off (PRE), followed immediately by (2) a 180-second acquisition during continuous laser stimulation (POST). The laser remained off during the baseline period and was activated only during the POST recording. All physiological parameters—including respiration rate, heart rate, and maximal recorded temperature—were collected during each 180-second interval.

Standard parasternal long-axis (B-mode) and short-axis (M-mode) two-dimensional brightness mode images were acquired to visualize left ventricular (LV) structure. Targeted M-mode recordings at the mid-papillary short-axis level were used to quantify systolic functional indices, including fractional shortening (FS%; measurement reflecting the contractile ability of the LV) and M-mode ejection fraction (EF%; represents the percentage of blood ejected from the ventricle during each heartbeat relative to the volume present at the end of diastole and is used as an indicator of cardiac systolic function). Stroke volume (SV; measurement of the volume of blood ejected by the LV with each heartbeat, reflecting the LV pumping capacity) and cardiac output (CO; measurement of the total volume of blood pumped by the heart per minute, reflecting the ability of the cardiovascular system to meet the body's metabolic demands) were derived from VEVO-automated LV volume calculations using manufacturer-provided algorithms. All measurements were obtained from at least three consecutive cardiac cycles within each imaging period.

Stability of anesthesia was verified by maintaining temperature and heart rate within a physiologically appropriate range for lightly anesthetized mice. All echocardiographic analyses were performed offline.

2.8 AMG517-induced hyperthermia control

To determine whether increased body temperature alone was sufficient to reproduce the behavioral and cardiac effects observed following VMH→AHA photostimulation, a separate cohort of mice received systemic administration of AMG517. AMG517 was formulated at 1 mg/mL in saline containing 10% dimethyl sulfoxide (DMSO) and administered subcutaneously at 5 mg/kg. Control mice received the corresponding vehicle solution. AMG517 and vehicle-treated mice did not undergo optogenetic stimulation or laser exposure.

JNeurosci Accepted Manuscript

Body temperature was measured immediately prior to treatment and at 12, 24, and 30 min following administration. Maximum body temperature was also compared between treatment groups to confirm that AMG517 produced the intended hyperthermic response.

Following pharmacological treatment, mice underwent open-field, complex-escape, and elevated-plus-maze behavioral testing using the same behavioral outcome measures described above, with the exception that no mice were tethered to an optical fiber and no laser stimulation was delivered. Open-field measurements included total distance travelled, maximum speed, jumping behavior, freezing-bout number, time spent freezing, time immobile, center distance traveled, center entries, and time spent in the center zone. Complex-escape measurements included latency to escape and escape success. Elevated-plus-maze measurements included time spent in the open and closed arms, open- and closed-arm entries, distance traveled within the open and closed arms, total distance traveled, center entries, and head-dip entries.

A separate echocardiographic assessment was performed in saline and AMG517 treated mice using the VEVO 3100 Imaging System as described above. Animals were anesthetized with isoflurane and cardiac function was assessed without laser stimulation. Heart rate, fractional shortening, stroke volume, cardiac output, and M-mode ejection fraction were quantified to determine whether pharmacologically induced hyperthermia was sufficient to reproduce the cardiac effects observed following VMH→AHA photostimulation.

2.9 Euthanasia, blood, and tissue collection

Mice were deeply anesthetized. After snipping the right atrium, blood was collected using soda-lime glass micro-hematocrit capillary tubes that were sodium heparinized (Cat #: 51613, Globe Scientific, Mahwah, NJ) and deposited into heparinized tubes. Mice were then transcardially perfused with 1x phosphate-buffered saline (PBS) followed by 4% paraformaldehyde in 1x PBS or 10% formalin. Whole brains were removed and post-fixed in 4% paraformaldehyde in 1x PBS or 10% formalin for at least 24 hours before further processing. For all experiments, tissue was embedded in 2% agarose in PBS. 40 µm free-floating coronal brain sections were collected using a Precisionary Instruments vibratome (Precisionary Instruments VF-500-0Z, Precisionary Instruments LLC, Ashland, MA).

2.10 IL-6 Enzyme-linked immunosorbent assay

Plasma IL-6 enzyme-linked immunosorbent assay (ELISA) was conducted with Mouse ELISA Kit (Cat #: ELM-IL6-1, RayBiotech, Inc., Peachtree Corners, GA) in accordance with kit instructions. Samples were run in duplicate. Briefly, 100 µl of standard or sample was added to each well.

JNeurosci Accepted Manuscript

They were incubated for 2.5 hours at room temperature, followed by addition of 100 µl of biotin antibody to each well. They were incubated for 1 hour at room temperature, followed by the addition of 100 µl of Streptavidin solution to each well. The plate was incubated for 45 minutes at room temperature, followed by addition of 100 µl of TMB One-Step Substrate Reagent to each well. 50 µl of Stop Solution was added to each well and plates were read at 450 nm on a CLARIOstar Plus (BMG Labtech, Cary, NC).

2.11 Histological analysis and c-Fos immunostaining

For mCherry verification of transgene expression, all slices were mounted onto Superfrost glass slides (Cat # 22-037-246; VWR International, PA, USA) which were covered with Vectashield PLUS antifade mounting media with DAPI (Cat #: H-2000-2, Vector Laboratories Inc, Newark, CA) before imaging. DAPI and mCherry images were acquired with a Nikon T-100 using NIS-Elements software (Nikon Instruments Inc., Melville, NY).

For c-Fos immunostaining, 1 of every 12 brain slices was serially sampled. This resulted in one section that contained the AHA for each mouse, two to three sections that spanned the habenula/paraventricular thalamus, two to three sections that spanned the periaqueductal gray, and one section that spanned the locus coeruleus. For structures with multiple sections per structure, a per-animal average was calculated for analysis so that each data point represents an individual animal. Sections were washed in 1x PBS 6x for 10 minutes each. They were then blocked in PBST (1x phosphate-buffered saline + 0.3% Triton X-100) with 3% normal donkey serum for 1 hour at room temperature. Samples were then incubated in a tube on a rotomixer overnight in PBST plus 3% normal donkey serum and 1:500 dilution of phospho-c-Fos (Ser32)(D82C12) XP Rabbit mAb (Cat #: 5348, Cell Signaling Technology, Danvers, MA). The next day, slices were washed 6x for 10 minutes each. Samples were then placed into 1x PBST + 3% normal donkey serum, plus 1:500 donkey anti-rabbit highly cross-adsorbed 647 secondary antibody (Cat #: 32795, Invitrogen, Carlsbad, CA). Slices were washed 3x for 10 minutes each, mounted, and imaged as described above. For imaging analysis, approximately matched coronal sections were used for each of the structures analyzed. The value for each mouse (experimental unit) for each structure was calculated as the average across the measured slices (observational units). Regions were painted in accordance with relevant landmarks and cells were counted as c-Fos positive cells using semi-automated software named Brain Atlas Regional Cell Counter. Brain regions were applied using the paint feature to approximate Paxinos and Franklin Atlas boundaries. Detection parameters were optimized for each image using the “Smart Suggest” feature and then tuned to ensure that false positives and negatives were minimized. Accuracy

JNeurosci Accepted Manuscript

was further ensured by manually adding or subtracting from the mask to ensure that the detection was matching valid counts. All metadata, masked cell counts, and XY locations of cells were logged.

2.12 Statistical analysis

Statistical analysis was conducted in GraphPad Prism 11 (RRID:SCR_002798; GraphPad, La Jolla, CA, USA). All graphed data are represented as mean ± SEM (except for contingency tables of escape success). The number of experimental units is depicted as *n* for number of animals for each experiment, which are specified in the supplementary table of statistics **(Table S1)**. For each test, QQ plots and residual vs. fit plots were assessed. For all t-tests, if homogeneity of variance was violated, the Welch's correction was applied. For all two-way ANOVAs where there were four levels (OFF-ON-OFF-ON), Geisser-Greenhouse's Epsilon was checked and if that value was below 0.75, the Geisser-Greenhouse correction was made. Holm-Sidak corrected multiple comparisons were made in all cases where significant main or interaction effects were detected. For contingency table analysis, Fisher's Exact Test was employed. This was selected over the Chi-squared test because of the relatively low numbers in the Control group success category and the ChR2 group fail category.

3. Results

3.1 Validation of channelrhodopsin-2 expression in experimental mice

We selectively targeted the VMH in SF1-Cre mice with an adeno-associated virus (AAV) that has channelrhodopsin-2 (ChR2) and mCherry transgenes flanked by heterotypic lox sites and implanted fiber optics dorsal to the AHA. We visualized this mCherry signal with fluorescent microscopy to verify expression in the VMH for each mouse in the study **(Fig. 1B)**, and to visualize axons in the AHA **(Fig. 1C)**. Mice were excluded if they had a positive PCR for the Cre recombinase gene and no visible mCherry signal. No mice that had a negative PCR test showed visible mCherry signal.

3.2 Increased maximum speed and jumping behavior during VMH→AHA stimulation in mice

For the open field test, we did not detect any significant differences in distance traveled during VMH^{SF1}:ChR2→AHA stimulation **(Fig. 2A)**. However, we did detect significant increases in maximum speed in VMH^{SF1}:ChR2→AHA mice during the stimulation compared to the control group **(Fig. 2B)**. In addition, we observed a significant interaction effect for transgene and bin between groups for number of jumps **(Fig. 2C)**. We did not observe any significant differences in

JNeurosci Accepted Manuscript

freezing behavior **(Fig. 2D)** or time spent freezing **(Fig. 2E)**. Notably, we did not observe any group or stimulation effects on time immobile **(Fig. 2F)**. We next examined center zone exploration during photostimulation. We detected no significant group differences in overall center distance traveled **(Fig. 2G)**. However, there was a significant bin by transgene interaction in center entries **(Fig. 2H)**. For center entries, multiple comparisons revealed that VMH→AHA mice had significantly fewer center zone entries during their second OFF bin than the first OFF bin. For time in center, no significant main or interaction effects were detected **(Fig. 2I)**.

3.3 Reduced latency to escape in VMH→AHA stimulated mice

We sought to test whether mice exhibit complex escape during VMH→AHA stimulation. Immediately following the open field test, a wire grid ladder was placed in the apparatus to create a three-dimensional escape route. The first three minutes of the complex escape task were without laser stimulation, and zero mice escaped the apparatus. Next, a three-minute laser ON bin occurred. During this period, VMH^{SF1}:ChR2→AHA mice exhibited a significantly shorter latency to escape **(Fig. 3B)**. In addition, significantly more VMH^{SF1}:ChR2→AHA stimulated mice escaped the apparatus compared to control mice **(Fig. 3C)**.

3.4 Increased anxiety-like behavior on the elevated plus maze following VMH→AHA stimulation

We sought to test whether the state instantiated by VMH^{SF1}:ChR2→AHA stimulation persisted beyond the delivery of illumination. To do this, we used the elevated plus maze to test the anxiety-like behavior of mice. Mice were stimulated in their open field test chamber for 3 minutes and then moved to an adjacent room for elevated plus maze testing. We observed no change in time in open arms between groups **(Fig. 4A)**, a significant decrease in open arms entries **(Fig. 4B)** in VMH^{SF1}:ChR2→AHA mice compared to controls, and no change in open arms distance **(Fig. 4C).** Importantly, we observed that VMH^{SF1}:ChR2→AHA mice had significantly greater time in closed arms **(Fig. 4D)**, but not any significant changes in closed arms entries **(Fig. 4E)** or closed arms distance **(Fig. 4F)**. We also did not observe any significant differences between groups for distance traveled **(Fig. 4G)**, center zone entries **(Fig. 4H)**, or head dip entries **(Fig. 4I)**. These results together indicate that increased anxiety-like behavior is sustained following VMH^{SF1}:ChR2→AHA stimulation. This is consistent with previous results that show VMH neurons drive state changes rather than encode specific behaviors(Kennedy et al., 2020).

3.5 Increased heart rate and fractional shortening in anesthetized VMH→AHA stimulated mice

Neurosci Accepted Manuscript

VMH^{SF1}:ChR2→AHA stimulation produced selective physiological and cardiac alterations as assessed by echocardiography **(Fig. 5A)** before and during photoactivation. Respiration rate was unchanged between PRE and POST exposure in both groups **(Fig. 5B)**, indicating that VMH^{SF1}:ChR2→AHA stimulation did not induce measurable ventilatory changes under anesthesia. In contrast, maximum core temperature was significantly different between groups during the stimulation phase **(Fig. 5C)**, indicating that inadvertent hypothermia caused by the duration of anesthesia was offset by stimulation. The increase is consistent with output from VMH^{Pdyn} neurons to increase thermogenesis(Feng et al., 2022).

Representative B-mode imaging **(Fig. 5D)** shows preserved left ventricular morphology without evidence of acute structural disturbance. Quantitative functional analysis revealed a significant change in heart rate in the VMH^{SF1}:ChR2→AHA group at the post timepoint relative to control **(Fig. 5E)**, suggesting a VMH^{SF1}:ChR2→AHA stimulation-induced elevation in autonomic cardiac activation.

Systolic performance was enhanced by VMH^{SF1}:ChR2→AHA stimulation, as evidenced by an increase in fractional shortening (FS%; measurement reflecting the contractile ability of the left ventricle) **(Fig. 5F)**. Despite this improvement in contractile index, stroke volume (SV; measurement of the volume of blood ejected by the left ventricle with each heartbeat reflecting the left ventricle pumping capacity) remained unchanged between PRE and POST conditions in the VMH^{SF1}:ChR2→AHA stimulation group and was elevated in the control group **(Fig. 5G)**, indicating that the contractile enhancement did not translate to increased volume ejection per beat from VMH^{SF1}:ChR2→AHA stimulation.

No changes were detected in cardiac output (CO; measurement of the total volume of blood pumped by the heart per minute reflecting the ability of the cardiovascular system to meet the body's metabolic demands) between or within groups **(Fig. 5H)**, despite elevated HR in the VMH^{SF1}:ChR2→AHA stimulation group compared to controls. This is partially because SV was unaffected in the VMH^{SF1}:ChR2→AHA stimulation group while increased in the controls. M-mode–derived ejection fraction (EF%; represents the percentage of blood ejected from the ventricle during each heartbeat relative to the volume present at the end of diastole and is used as an indicator of cardiac systolic function) similarly showed no significant difference between PRE and POST application **(Fig. 5I)**, indicating that the variability induced by the anesthesia was sufficient to mask any relatively minor global systolic changes.

JNeurosci Accepted Manuscript

Together, these findings indicate that acute VMH^{SF1}:ChR2→AHA stimulation increases heart rate and enhances fractional shortening. This profile matches a selective improvement in contractile kinetics rather than changes in overall volumetric cardiac function.

3.6 Increased circulating IL-6 in VMH→AHA stimulated mice

Acute stress is known to increase IL-6 secretion by brown adipocytes in mice, which makes them susceptible to infections(Qing et al., 2020). This effect is attenuated by ablation of sympathetic neurons. However, it is unknown whether circulating IL-6 is increased by hypothalamic defense network activation independent of any environmental stressor. Thus, we tested the effect of one hour of VMH^{SF1}:ChR2→AHA photostimulation on circulating IL-6 levels. We found that they are significantly increased following stimulation **(Fig. 6A)**. This finding indicates that VMH^{SF1}:ChR2→AHA photoactivation is sufficient to generate an acute pro-inflammatory state that regulates and promotes hyperglycemia during stress exposure as part of the activation of fight or flight mechanisms.

3.7 VMH→AHA stimulation increases activity in the lateral habenula, anterior hypothalamic area, ventral premammillary nucleus, ventrolateral periaqueductal gray, and locus coeruleus

Numerous circuit node diagrams have been proposed to link exposure of mammals to environmental factors with observable changes in activity patterns, behavior, and physiology. While these approaches have been useful, they often are unable to isolate the consequences of individual projections because of the feedback loops that underlie functions that are so critical for fitness. Thus, we set out to check for changes in activity patterns of brain regions known to be involved in relaying avoidance behavior, three-dimensional escape, and physiological arousal using c-Fos immunostaining of the lateral habenula(Pobbe and Zangrossi Jr, 2010; Vincenz et al., 2017), dorsal premammillary nucleus (Wang et al., 2015), and the locus coeruleus (Liu et al., 2024; Nassar, 2024). We photostimulated for one hour before euthanasia, extracted brains, and conducted c-Fos immunostaining. We found a significant elevation of c-Fos immunostaining in the anterior hypothalamic area of VMH^{SF1}:ChR2→AHA stimulated mice. This activity change would support avoidance behavior and processing of aversive stimuli (Groos and Helmchen, 2024). PMd c-Fos expression did not have a sufficiently low false discovery rate when accounting for multiple comparisons (t_7 = 2.522, p = 0.0397, q = 0.0860) even though the stand-alone t-test was significant. PMd activation is consistent with the behavioral observation of complex escape (Wang et al., 2021b) and c-Fos expression patterns following exposure to predators (Cezario et al., 2008). We observed significantly increased activation of the PMv, which is also implicated in

Neurosci Accepted Manuscript

social (de Almeida et al., 2022) and maternal aggression (Motta et al., 2013). In addition, we observed significant increases in the vlPAG in VMH^{SF1}:ChR2→AHA stimulated mice compared to fluorophore controls. Finally, we observed a significant increase in locus coeruleus c-Fos expression **(Fig. 7B).** Locus coeruleus activity facilitates defensive responses to looming stimuli (Li et al., 2018), orientation to task-related environmental stimuli (Berridge and Waterhouse, 2003), and fear-induced suppression of feeding (Wainstein et al., 2022).

3.8 Increased body temperature induced by AMG517 does not cause complex escape behavior, anxiety-like behavior, or significant changes in cardiac function

We sought to determine if the changes observed following VMH^{SF1}:ChR2→AHA stimulation were a secondary result of change in body temperature. To test this, we administered a dose of AMG517 known to increase body temperature and test the mice for changes in echocardiography, open field test, complex escape task, elevated plus maze. We tested the mice for body temperature **(Figure 8A)** change following AMG517 administration and found a significant increase in maximum **(Figure 8B)** and average body temperature compared to control mice **(Figure 8C)**. We then tested these mice for cardiac changes with echocardiography and found no significant differences in heart rate **(Figure 8D)**, fractional shortening **(Figure 8E)**, stroke volume **(Figure 8F)**, cardiac output **(Figure 8G)**, or ejection fraction **(Figure 8H)**.

When we tested these mice for behavioral differences in the open field test, we found no significant differences in distance traveled **(Figure 9A)**, maximum speed **(Figure 9B)**, jumps **(Figure 9C)**, Freezing bouts **(Figure 9D)**, time spent freezing **(Figure 9E)**, time immobile **(Figure 9F)**, center distance **(Figure 9G)**, center entries **(Figure 9H)**, or time in center **(Figure 9I)**. When we tested these mice in the complex escape task, there were no significant differences for latency to escape and no AMG517 mice escaped the apparatus and one saline mouse escaped the apparatus **(Figure 9K)**. Of note, we ran this test for 12 minutes which was 4x as long as the ON epoch of the complex escape test during VMH^{SF1}:ChR2→AHA stimulation.

Finally, in the elevated plus maze we did not detect any significant differences between control and AMG517 treated mice for time in open arms **(Figure 9L)**, open arm entries **(Figure 9M)**, open arms distance **(Figure 9N)**, time in closed arms **(Figure 9O)**, closed arm entries **(Figure 9P)**, closed arms distance **(Figure 9Q)**, distance traveled **(Figure 9R)**, center entries **(Figure 9S)**, or head dip entries **(Figure 9T)**. Taken together, these experiments dissociated the observations from VMH^{SF1}:ChR2→AHA stimulation and change in body temperature.

4. Discussion

JNeurosci Accepted Manuscript

These results show for the first time that ventromedial hypothalamus to anterior hypothalamic area (VMH→AHA) projections contribute to the orchestration of complex behavioral escape in which mice navigate a three-dimensional route out of the apparatus. Following VMH^{SF1}→AHA stimulation, mice exhibit elevated anxiety-like behavior on the elevated plus maze. VMH^{SF1}→AHA stimulation also evoked changes in temperature, cardiac physiology, and circulating cytokine levels that are known features of threat responding. In the context of the predator imminence continuum, this work demonstrates that the VMH^{SF1}→AHA projection can trigger early circa-strike escape.

While research has tested VMH soma stimulation in SF1-Cre mice in a complex escape task(Wang et al., 2021b), those authors report that the VMH doesn't elicit context-specific escape. In that seminal work, only one mouse escaped during VMH^{SF1} stimulation, while PMd^{CCK} stimulation caused every mouse to escape. The proportion of mice that escaped the apparatus here is approximately 50%, which is less than PMd^{CCK} activation. The complexity of navigation route may explain this difference. Alternatively, their soma activation of the VMH may activate collaterals that cause freezing (Wang et al., 2015). Our data suggests that AHA activation has shifted behavioral selection towards complex escape. This is consistent with the AHA projections to the PMd observed by us (Laing et al., 2023) and others (Saper et al., 1978). This indicates that VMH^{SF1}:ChR2→AHA stimulation generates complex escape behavior aligned with the behavior observed during PMd activation by DREADDs (Wang et al., 2021a).

Optogenetic activation of anxiogenic circuits is often on the elevated plus maze (Tye et al., 2011), but for this circuit mice jump off of the apparatus. We opted to stimulate the mice in the open field apparatus, untether them, and then place them on the elevated plus maze. Our data indicate that anxiety-like behavior in the stimulated mice was increased compared to controls, which suggests a shift in state beyond circa-strike motor plan execution. Further testing will be needed to understand whether circumstances dictate the transition to pathological anxiety by changes in VMH^{SF1}→AHA activity.

The echocardiographic studies here were conducted in anesthetized animals to extend findings that VMH stimulation increased sympathetic effects on the heart (Wang et al., 2015) to determine whether perception was required for the detection of peripheral effects. The findings that heart rate was elevated by VMH^{SF1}:ChR2→AHA stimulation compared to controls, combined with an increase in fractional shortening clarified that the VMH^{SF1}→AHA projection causes cardiac effects consistent with sympathetic arousal even in the absence of perception. This reflects a one-dimensional mid-cavity diameter change of an autonomically sensitive index. Previous positive

JNeurosci Accepted Manuscript

associations between fractional shortening and anxiety have been reported (Soghyani et al., 2025). It is likely that global ejection fraction changes are buffered by geometry, afterload, and heart rate, given that these are healthy animals experiencing acute stimulation. Future studies should test the effects of chronic VMH^{SF1}:ChR2→AHA stimulation on cardiac function by echocardiography to determine whether it is sufficient to drive remodeling, or whether inhibition of VMH→AHA activation during stress can prevent cardiac remodeling. As part of echocardiographic studies, we monitored the temperature of the mice and found that the body temperature of VMH^{SF1}:ChR2→AHA stimulated mice was significantly higher than controls. The increase is consistent with output from VMH^{Pdyn} neurons to increase thermogenesis(Feng et al., 2022). This is also consistent with reports of increases in body temperature that follow handling stress (Blenkuš et al., 2022). Stress-induced increases in body temperature are attributable to release of norepinephrine onto brown adipose tissue that activates uncoupling protein 1 (Cannon and Nedergaard, 2004), which can be blocked by β3 antagonism (Lkhagvasuren et al., 2011). To a lesser extent, cutaneous vasoconstriction(Nakamura, 2015) also contributes. Our findings here identify increased temperature as a feature downstream of VMH^{SF1}→AHA activation.

Restraint stress increases release of corticosterone that is dependent on AHA activity(Bang et al., 2022). Restraint stress increases circulating levels of IL-6 (Shizuya et al., 1997; Voorhees et al., 2013) that is dependent on sympathetic output to brown-adipose tissue (Qing et al., 2020). IL-6 levels are increased in anxious human patients as measured by the Hospital Anxiety and Depression Scale (O'Donovan et al., 2010). In the context of acute threat responding, increased IL-6 promotes host defense against infection and blood coagulation in the event of injury (Narazaki and Kishimoto, 2018) as well as blood glucose availability, but this occurs at the cost of decreased host fitness to subsequent inflammatory challenge (Qing et al., 2020). Here, the coincident increase in circulating IL-6 is surmised to provide two significant benefits during escape via increased glucose substrate availability for muscles that actuate locomotion and blood coagulation in the event of injury during failed escape. Future work should determine whether prolonged AHA activation decreases host fitness, or whether AHA inhibition during stress exposure can prevent inflammation. These experiments may inform human disease susceptibility under prolonged stress (Papanicolaou et al., 1998). These IL-6 findings are consistent with the locus coeruleus activation following VMH^{SF1}:ChR2→AHA stimulation and known mediation of IL-6 secretion by catecholamines (Johnson et al., 2005).

The c-Fos analysis demonstrates that in vivo activation of the AHA via activation of VMH projections. This activation is consistent with glutamate release from excitatory VMH neurons

JNeurosci Accepted Manuscript

(Laing et al., 2025). The c-Fos analysis of downstream brain regions contextualizes the findings of VMH^{SF1}:ChR2→AHA stimulation of defensive behavior and physiology. While the PMd activation effect did not survive multiple comparisons corrections due to the large number of structures analyzed, it was *a priori* as a candidate target downstream of AHA activation. PMd neurons are reported to become activated by threat exposure and suppress hunger states (de Araujo Salgado and Krashes, 2026) and AgRP population dynamics (de Araujo Salgado et al., 2023). Further, thyrotropin releasing hormone activates PMd neurons and increases darting behavior (Coletta and Laing, 2026). This effect is consistent with the complex escape phenotype and indicates the importance of future studies into the role of VMH→AHA activity in learned escape behavior (Torossian et al., 2025). The VMH, AHA, and PMd are well known to form an excitatory network (Hong and Kim).

The effect of PMv activation that we observed here is interesting given the functions of the PMv to control autonomic arousal, but also that activation of the PMv is reported control freezing in opposition to flight. PMv neurons also send efferent projections to the AHA (Xie et al., 2022). It is possible that the c-Fos immunostaining here may reflect activation of counterregulatory populations that support maintaining balance between these survival behaviors and is not to be taken as direct activation of the PMv by the AHA. Future work should further elucidate the extent to which joint PMd and PMv activation contributes to the regulatory balance of selection between fight, flight, and freezing (Mongeau et al., 2003) as part of a complex network. The lateral habenula is reported to drive avoidance behavior (Stamatakis and Stuber, 2012). This can negatively reinforce behavioral responding by post-synaptic potentiation of AMPAR-dependent transmission onto lateral habenula neurons (Trusel et al., 2019). Elevated locus coeruleus c-Fos expression in the experimental group matches the behavioral and cardiac phenotypes we observed. The increase in an anxiety-like state during the elevated plus maze may be partially attributable to the locus coeruleus changes, which would match associations that are conserved in humans(Bachman et al., 2022). The PAG findings here showed elevated c-Fos expression in the vlPAG, though we did not see a significant elevation of dorsolateral PAG. Future work should identify the molecularly defined populations that are activated downstream of the VMH^{SF1}→AHA projection.

The studies reported here have a few limitations. First, it is plausible that the some of effects observed are dependent on the VMH and not the AHA. Given the relative lack of freezing behavior we observe, it is unlikely that off-target or antidromic stimulation is activating collateral projections. Thus, we think this limitation has minimal influence on our findings. We did not

JNeurosci Accepted Manuscript

formally test mechanical attack with an object. It is possible that under certain contexts or housing conditions this behavior is observable, but we did not observe noteworthy aggression from mice (Xie et al., 2022). In addition, the echocardiography studies here were limited by the anesthesia effects on peripheral physiology and cardiac function, such as reduced temperature and a lowering of the heart rate. However, these studies were designed to have between-group comparisons to circumvent this. Finally, the c-Fos studies here were limited in total sampling through the tissue. Thus, these are approximately matched semi-quantitative relative differences between groups rather than absolute activity levels of structures. Future studies should analyze whole-brain connectome changes following stimulation.

In summary, here we report that activation of the VMH^{SF1}→AHA projection evokes complex escape behavior. Following stimulation, anxiety-like behavior remains increased on the elevated plus maze, changes in cardiac physiology in anesthetized mice independent of perception, and an evoked increase in IL-6. We found increases in activity patterns of numerous downstream brain regions such as AHA, PMv, LHab, vlPAG, and the LC. These findings point to this projection as a critical input to nodes involved in avoidance behavior, escape behavior, and physiological arousal.

Declaration of Interests

The authors declare no competing interests.

Acknowledgements

Grok artificial intelligence assisted in language editing and document proofing. All scientific decisions and analysis were completed and written by the authors of the manuscript.

References

Bachman SL, Nashiro K, Yoo H, Wang D, Thayer JF, Mather M (2022) Associations between locus coeruleus MRI contrast and physiological responses to acute stress in younger and older adults. Brain research 1796:148070.

Bang JY, Zhao J, Rahman M, St-Cyr S, McGowan PO, Kim JC (2022) Hippocampus-Anterior Hypothalamic Circuit Modulates Stress-Induced Endocrine and Behavioral Response. Frontiers in Neural Circuits Volume 16 - 2022.

Berridge CW, Waterhouse BD (2003) The locus coeruleus–noradrenergic system: modulation of behavioral state and state-dependent cognitive processes. Brain research reviews 42:33-84.

Bingham NC, Verma-Kurvari S, Parada LF, Parker KL (2006) Development of a steroidogenic factor 1/Cre transgenic mouse line. genesis 44:419-424.

JNeurosci Accepted Manuscript

Blanchard DC, Griebel G, Blanchard RJ (2001) Mouse defensive behaviors: pharmacological and behavioral assays for anxiety and panic. Neuroscience & Biobehavioral Reviews 25:205-218.
Blenkuš U, Gerós AF, Carpinteiro C, Aguiar PD, Olsson IAS, Franco NH (2022) Non-Invasive Assessment of Mild Stress-Induced Hyperthermia by Infrared Thermography in Laboratory Mice. In: Animals, p 177.
Cannon B, Nedergaard JAN (2004) Brown Adipose Tissue: Function and Physiological Significance. Physiological Reviews 84:277-359.
Cannon WB (1953) Bodily changes in pain, hunger, fear, and rage, ed2. Boston, CH Branford:20-36.
Cezario AF, Ribeiro-Barbosa ER, Baldo MVC, Canteras NS (2008) Hypothalamic sites responding to predator threats–the role of the dorsal premammillary nucleus in unconditioned and conditioned antipredatory defensive behavior. European Journal of Neuroscience 28:1003-1015.
Cheung KYM, Nair A, Li L-y, Shapiro MG, Anderson DJ (2025) Population coding of predator imminence in the hypothalamus. Neuron 113:1259-1275.e1254.
Claudi F, Campagner D, Branco T (2022) Innate heuristics and fast learning support escape route selection in mice. Current Biology 32:2980-2987.e2985.
Coletta CM, Laing BT (2026) Thyrotropin-Releasing Hormone Increases Dorsal Premammillary Nucleus Neuron Activity and Darting Behavior. Neuropharmacology:111223.
de Almeida AP, Baldo MVC, Motta SC (2022) Dynamics in brain activation and behaviour in acute and repeated social defensive behaviour. Proceedings of the Royal Society B: Biological Sciences 289:20220799.
de Araujo Salgado I, Krashes MJ (2026) High-fat food reinforces risk taking by suppressing defensive neurons. Current Biology 36:49-62.e44.
de Araujo Salgado I, Li C, Burnett CJ, Gonzalez SR, Becker JJ, Horvath A, Earnest T, Kravitz AV, Krashes MJ (2023) Toggling between food-seeking and self-preservation behaviors via hypothalamic response networks. Neuron 111:2899-2917.
Dhillon H, Zigman JM, Ye C, Lee CE, McGovern RA, Tang V, Kenny CD, Christiansen LM, White RD, Edelstein EA, Coppari R, Balthasar N, Cowley MA, Chua S, Jr., Elmquist JK, Lowell BB (2006) Leptin Directly Activates SF1 Neurons in the VMH, and This Action by Leptin Is Required for Normal Body-Weight Homeostasis. Neuron 49:191-203.
Feng C, Wang Y, Zha X, Cao H, Huang S, Cao D, Zhang K, Xie T, Xu X, Liang Z, Zhang Z (2022) Cold-sensitive ventromedial hypothalamic neurons control homeostatic thermogenesis and social interaction-associated hyperthermia. Cell Metabolism 34:888-901.e885.
Groos D, Helmchen F (2024) The lateral habenula: A hub for value-guided behavior. Cell reports 43.
Hong CY, Kim JC (2026) Re-evaluation of the medial hypothalamic defence system through a cell-type lens. Trends Open.
Johnson JD, Campisi J, Sharkey CM, Kennedy SL, Nickerson M, Greenwood BN, Fleshner M (2005) Catecholamines mediate stress-induced increases in peripheral and central inflammatory cytokines. Neuroscience 135:1295-1307.
Kennedy A, Kunwar PS, Li L-y, Stagkourakis S, Wagenaar DA, Anderson DJ (2020) Stimulus-specific hypothalamic encoding of a persistent defensive state. Nature 586:730-734.
Kunwar PS, Zelikowsky M, Remedios R, Cai H, Yilmaz M, Meister M, Anderson DJ (2015) Ventromedial hypothalamic neurons control a defensive emotion state. eLife 4:e06633.
Laing BT, Anderson MS, Bonaventura J, Jayan A, Sarsfield S, Gajendiran A, Michaelides M, Aponte Y (2023) Anterior hypothalamic parvalbumin neurons are glutamatergic and promote escape behavior. Current Biology 33:3215-3228.

JNeurosci Accepted Manuscript

Laing BT, Anderson MS, Jayan A, Park AS, Erbaugh LJ, Solis O, Wilson DJ, Michaelides M, Aponte Y (2025) Repetitive Grooming Behavior Following Aversive Stimulus Coincides with a Decrease in Anterior Hypothalamic Area Activity. eneuro 12:ENEURO.0417-0424.2024.
Li L, Feng X, Zhou Z, Zhang H, Shi Q, Lei Z, Shen P, Yang Q, Zhao B, Chen S (2018) Stress accelerates defensive responses to looming in mice and involves a locus coeruleus-superior colliculus projection. Current Biology 28:859-871.
Lindsey ML, Kassiri Z, Virag JAI, de Castro Brás LE, Scherrer-Crosbie M (2018) Guidelines for measuring cardiac physiology in mice. American Journal of Physiology-Heart and Circulatory Physiology 314:H733-H752.
Liu J, Lustberg DJ, Galvez A, Liles LC, McCann KE, Weinshenker D (2024) Genetic disruption of dopamine β-hydroxylase dysregulates innate responses to predator odor in mice. Neurobiology of Stress 29:100612.
Lkhagvasuren B, Nakamura Y, Oka T, Sudo N, Nakamura K (2011) Social defeat stress induces hyperthermia through activation of thermoregulatory sympathetic premotor neurons in the medullary raphe region. European Journal of Neuroscience 34:1442-1452.
Mongeau R, Miller GA, Chiang E, Anderson DJ (2003) Neural Correlates of Competing Fear Behaviors Evoked by an Innately Aversive Stimulus. The Journal of Neuroscience 23:3855.
Motta SC, Guimarães CC, Furigo IC, Sukikara MH, Baldo MVC, Lonstein JS, Canteras NS (2013) Ventral premammillary nucleus as a critical sensory relay to the maternal aggression network. Proceedings of the National Academy of Sciences 110:14438-14443.
Nakamura K (2015) Neural circuit for psychological stress-induced hyperthermia. Temperature 2:352-361.
Narazaki M, Kishimoto T (2018) The Two-Faced Cytokine IL-6 in Host Defense and Diseases. In: International Journal of Molecular Sciences, p 3528.
Nassar MR (2024) Toward a computational role for locus coeruleus/norepinephrine arousal systems. Current Opinion in Behavioral Sciences 59:101407.
O'Donovan A, Hughes BM, Slavich GM, Lynch L, Cronin M-T, O'Farrelly C, Malone KM (2010) Clinical anxiety, cortisol and interleukin-6: Evidence for specificity in emotion–biology relationships. Brain, behavior, and immunity 24:1074-1077.
Papanicolaou DA, Wilder RL, Manolagas SC, Chrousos GP (1998) The pathophysiologic roles of interleukin-6 in human disease. Annals of internal medicine 128:127-137.
Pobbe RLH, Zangrossi Jr H (2010) The lateral habenula regulates defensive behaviors through changes in 5-HT-mediated neurotransmission in the dorsal periaqueductal gray matter. Neuroscience letters 479:87-91.
Qing H, Desrouleaux R, Israni-Winger K, Mineur YS, Fogelman N, Zhang C, Rashed S, Palm NW, Sinha R, Picciotto MR, Perry RJ, Wang A (2020) Origin and Function of Stress-Induced IL-6 in Murine Models. Cell 182:372-387.e314.
Qrareya AN, Wise NS, Hodges ER, Mahdi F, Stewart JA, Paris JJ (2022) HIV-1 Tat Upregulates the Receptor for Advanced Glycation End Products and Superoxide Dismutase-2 in the Heart of Transgenic Mice. In: Viruses, p 2191.
Saper CB, Swanson LW, Cowan WM (1978) The efferent connections of the anterior hypothalamic area of the rat, cat and monkey. Journal of Comparative Neurology 182:575-599.
Shizuya K, Komori T, Fujiwara R, Miyahara S, Ohmori M, Nomura J (1997) The influence of restraint stress on the expression of mRNAs for IL-6 and the IL-6 receptor in the hypothalamus and midbrain of the rat. Life sciences 61:PL135-PL140.

JNeurosci Accepted Manuscript

Soghyani D, Arfaee F, Molazem M, Soflaei R, Abdous A (2025) The impact of anxiety on canine heart function: a study using echocardiographic techniques. BMC Veterinary Research 21:605.
Stamatakis AM, Stuber GD (2012) Activation of lateral habenula inputs to the ventral midbrain promotes behavioral avoidance. Nature neuroscience 15:1105-1107.
Torossian A, Miranda BA, Reis FMCV, Hilgert EL, Gudipati R, Bloom CPV, Wang W, Schuette PJ, Adhikari A (2025) Hypothalamic Control of Learned Flight Induced by Threat Imminence. The Journal of Neuroscience 45:e1806242025.
Trusel M, Nuno-Perez A, Lecca S, Harada H, Lalive AL, Congiu M, Takemoto K, Takahashi T, Ferraguti F, Mameli M (2019) Punishment-Predictive Cues Guide Avoidance through Potentiation of Hypothalamus-to-Habenula Synapses. Neuron 102:120-127.e124.
Tye KM, Prakash R, Kim S-Y, Fenno LE, Grosenick L, Zarabi H, Thompson KR, Gradinaru V, Ramakrishnan C, Deisseroth K (2011) Amygdala circuitry mediating reversible and bidirectional control of anxiety. Nature 471:358-362.
Vincenz D, Wernecke KEA, Fendt M, Goldschmidt J (2017) Habenula and interpeduncular nucleus differentially modulate predator odor-induced innate fear behavior in rats. Behavioural Brain Research 332:164-171.
Voorhees JL, Tarr AJ, Wohleb ES, Godbout JP, Mo X, Sheridan JF, Eubank TD, Marsh CB (2013) Prolonged restraint stress increases IL-6, reduces IL-10, and causes persistent depressive-like behavior that is reversed by recombinant IL-10. PloS one 8:e58488.
Wainstein G, Müller EJ, Taylor N, Munn B, Shine JM (2022) The role of the locus coeruleus in shaping adaptive cortical melodies. Trends in Cognitive Sciences 26:527-538.
Wang L, Chen Irene Z, Lin D (2015) Collateral Pathways from the Ventromedial Hypothalamus Mediate Defensive Behaviors. Neuron 85:1344-1358.
Wang W, Schuette PJ, La-Vu MQ, Torossian A, Tobias BC, Ceko M, Kragel PA, Reis FMCV, Ji S, Sehgal M, Maesta-Pereira S, Chakerian M, Silva AJ, Canteras NS, Wager T, Kao JC, Adhikari A (2021a) Dorsal premammillary projection to periaqueductal gray controls escape vigor from innate and conditioned threats. eLife 10:e69178.
Wang W, Schuette PJ, Nagai J, Tobias BC, Cuccovia V. Reis FM, Ji S, de Lima MAX, La-Vu MQ, Maesta-Pereira S, Chakerian M, Leonard SJ, Lin L, Severino AL, Cahill CM, Canteras NS, Khakh BS, Kao JC, Adhikari A (2021b) Coordination of escape and spatial navigation circuits orchestrates versatile flight from threats. Neuron 109:1848-1860.e1848.
Xie Z, Gu H, Huang M, Cheng X, Shang C, Tao T, Li D, Xie Y, Zhao J, Lu W, Zhang Z, Zhan C, Tang Z, Zhang F, Cao P (2022) Mechanically evoked defensive attack is controlled by GABAergic neurons in the anterior hypothalamic nucleus. Nature Neuroscience 25:72-85.

JNeurosci Accepted Manuscript

662

663

664

JNeurosci Accepted Manuscript

Figures

Figure 1: Overview of experimental manipulation and procedures. (A) Schematic representation of the experimental approach showing unilateral injection of AAV-FLEX-ChR2-mCherry into the ventromedial hypothalamus (VMH) of SF1-Cre mice and implantation of an optical fiber dorsal to the anterior hypothalamic area (AHA). **(B)** Representative coronal brain section showing mCherry expression localized to the VMH. **(C)** Representative coronal brain section showing mCherry-labeled VMH axon terminals within the AHA and the location of the implanted optical fiber.

JNeurosci Accepted Manuscript

Figure 2: VMH→AHA stimulation increases open field test maximum speed and jumping behavior. Gray bars indicated control group and blue bars indicate ChR2 experimental group (Ctrl n = 17 mice with 6 males and 11 females, ChR2 n = 12 total with 8 males and 4 females). **(A)** No significant differences were detected between groups for distance traveled (two-way ANOVA, Bin × Transgene: $F_{(1.327,35.83)} = 2.654$, $p = 0.1026$). **(B)** Significantly increased maximum speed for both bins of laser On in VMH→AHA group compared to controls (two-way ANOVA, Bin × Transgene: $F_{(3,81)} = 7.540$, $p = 0.0002$; On1 Ctrl vs. ChR2: $p < 0.0001$; On2 Ctrl vs. ChR2: $p < 0.0001$). **(C)** Significantly different number of jumps was detected (two-way ANOVA, Bin × Transgene: $F_{(1.037,28.01)} = 4.352$, $p = 0.0449$; Bin: $F_{(1.037,28.01)} = 4.352$, $p = 0.0449$; Transgene: $F_{(1,27)} = 4.899$, $p = 0.0355$; Mouse: $F_{(27, 81)} = 2.141$, $p = 0.0047$). **(D)** No significant differences were detected between groups for freezing bout number (two-way ANOVA, Bin × Transgene: $F_{(1.297,35.01)} = 1.123$, $p = 0.3134$). **(E)** No significant differences were detected between groups for time spent freezing (two-way ANOVA, Bin × Transgene: $F_{(1.568,42.35)} = 1.518$, $p = 0.2314$). **(F)** No significant differences were detected between groups for time immobile (two-way ANOVA, Bin × Transgene: $F_{(3,81)} = 1.943$, $p = 0.1292$). **(G)** No significant differences in center distance traveled were observed (two-way ANOVA, Bin × Transgene: $F_{(2.046,55.25)} = 0.8615$, $p = 0.4303$). **(H)** Significant differences were detected for center entries (two-way ANOVA, Bin x Transgene: $F_{(2.121,57.26)} = 4.114$, $p = 0.0195$; Bin: $F_{(2.121, 57.26)} = 6.395$, $p = 0.0026$; Transgene $F_{(1, 27)} = 0.1481$, $p = 0.7034$; ChR2 OFF1 vs OFF2: $p = 0.0268$). **(I)** No significant differences were observed for time in center between groups (Two-Way ANOVA, Bin x Transgene $F_{(3, 81)} = 0.3607$, $p = 0.7815$, Bin $F_{(3, 81)} = 1.148$, $p = 0.3349$, Transgene $F_{(1, 27)} = 0.0321$, $p = 0.8593$).

JNeurosci Accepted Manuscript

Figure 3: VMH→AHA stimulation evokes complex escape behavior. (A) Cartoon rendering of mouse with optogenetic stimulation climbing out of an apparatus on a wire grid in the complex escape task. **(B)** Significantly reduced latency to escape in VMH→AHA group compared to controls (Welch's corrected unpaired t-test, $t_{10} = 3.494$, $p = 0.0058$, **(C)** Significantly different proportion of escape success in VMH→AHA mice compared to controls (Fisher's exact test, $p = 0.0051$). For complex escape, groups included the same mice for all analysis (Ctrl n = 16 mice with 6 males and 10 females, ChR2 n = 11 total with 8 males and 3 females).

JNeurosci Accepted Manuscript

Figure 4: Anxiety-like behavior is increased on the elevated plus maze following VMH→AHA stimulation. (A) No significant differences were detected between groups for time in open arms (unpaired t-test, $t_{26} = 2.034$, $p = 0.0523$). **(B)** Significantly reduced open arms entries (unpaired t-test, $t_{26} = 3.286$, $p = 0.0029$) for the VMH→AHA group compared to controls. **(C)** No significant differences were detected between groups for open arms distance (unpaired t-test, $t_{26} = 1.717$, $p = 0.0979$). **(D)** Significantly increased time in closed arms in VMH→AHA group compared to control animals (unpaired t-test, $t_{26} = 2.491$, $p = 0.0195$). **(E)** No significant differences were detected between groups for closed arms entries (unpaired t-test, $t_{26} = 1.850$, $p = 0.0757$). **(F)** No significant differences were detected between groups for closed arms distance (unpaired t-test, $t_{26} = 1.204$, $p = 0.2395$). **(G)** No significant differences were detected between groups for total distance traveled (unpaired t-test, $t_{26} = 1.094$, $p = 0.2841$). **(H)** No significant differences were detected between groups for center entries (Welch's corrected unpaired t-test, $t_{12.25} = 1.594$, $p = 0.1364$). **(I)** No significant differences were detected between groups for head dip entries (unpaired t-test, $t_{26} = 0.5441$, $p = 0.5910$). For elevated plus maze, groups included the same mice for all analysis (Ctrl n = 17 mice with 6 males and 11 females, ChR2 n = 11 total with 7 males and 4 females).

JNeurosci Accepted Manuscript

Figure 5: VMH→AHA stimulation increases heart rate and fractional shortening. (A) Schematic of experimental design showing echocardiogram machine, isoflurane anesthetized mouse, laser diode, and timeline of 180s laser Off and 180s laser On periods. **(B)** No significant differences between or within groups were detected for respiration rate (two-way ANOVA, Stim × Transgene: $F_{(1,26)} = 1.420$, $p = 0.2442$). **(C)** Significantly higher max temperature was measured for the VMH→AHA group during the post-test stage (two-way ANOVA, Stim × Transgene: $F_{(1,27)} = 5.703$, $p = 0.0242$; Post Ctrl vs. ChR2: $p = 0.0054$). **(D)** Representative image of echocardiogram and heart rate signal. **(E)** Significantly higher heart rate beats per minute was measured for the VMH→AHA group during the post-test stage (two-way ANOVA, Stim × Transgene: $F_{(1,27)} = 4.762$, $p = 0.0380$; Post Ctrl vs. ChR2: $p = 0.0034$). **(F)** Significantly higher fractional shortening was measured for the post-test VMH→AHA group compared to their pre-test and controls during the post-test stage (two-way ANOVA, Stim × Transgene: $F_{(1,27)} = 8.314$, $p = 0.0076$; Post Ctrl vs. ChR2: $p = 0.0099$; ChR2 Pre vs. Post: $p = 0.0018$). **(G)** The control group had significantly elevated stroke volume (two-way ANOVA, Stim × Transgene: $F_{(1,27)} = 4.917$, $p = 0.0352$, Ctrl PRE vs POST $p = 0.0011$). **(H)** No significant differences were detected for either group for cardiac output (two-way ANOVA, Stim × Transgene: $F_{(1,27)} = 0.0411$, $p = 0.8409$). **(I)** No significant differences were detected for either group for M-mode ejection fraction (two-way ANOVA, Stim × Transgene: $F_{(1,27)} = 3.404$, $p = 0.0760$). For echocardiograph experimentation mice were used after the behavior experiments (control n = 17 mice, 6 males and 11 females, ChR2 n= 12 total with 8 males and 4 females).

JNeurosci Accepted Manuscript

Figure 6: VMH→AHA stimulation increases circulating IL-6 levels. (A) A significant increase in IL-6 levels following one hour of photostimulation of VMH→AHA projections (blue) compared to control (gray) (Welch's corrected unpaired t-test, $t_{7.1} = 2.709$, $p = 0.0298$, n = 7 ChR2 males, n = 5 CTRL males).

JNeurosci Accepted Manuscript

Figure 7: VMH→AHA stimulation increases c-Fos expression in the anterior hypothalamic area, lateral habenula, ventrolateral periaqueductal gray, and locus coeruleus. (A) Representative images of control (top panel) and VMH→AHA stimulated brain slices (bottom panel) across analyzed brain regions (*scale = 500 μm*). From left to right, the images correspond to those containing the anterior hypothalamic area (AHA) and paraventricular nucleus of the hypothalamus (PVN) in *column 1*, the medial habenula (MHab), lateral habenula (LHab), and paraventricular nucleus of the thalamus (PVT) in *column 2*, the dorsal premammillary nucleus, ventral premammillary nucleus and the arcuate (ARC) in *column 3*, the locus coeruleus (LC) in *column 4*, and the dorsomedial periaqueductal gray (dmPAG), dorsolateral periaqueductal gray (dlPAG), lateral periaqueductal gray (lPAG), and ventrolateral periaqueductal gray (vlPAG) in *column 5.* **(B)** Significantly elevated counts of c-Fos in AHA ($T_8 = 3.068$, $q = 0.0400$), PMv ($T_6 = 3.677$, $q = 0.0349$), LHab ($T_8 = 3.306$, $q = 0.0350$), LC ($T_8 = 12.52$, $q < 0.0001$), and vlPAG ($T_7 = 10.68$, $q < 0.0001$) of VMH→AHA mice compared to controls. No significant differences were detected for PVN ($T_8 = 0.7113$, $q = 0.5875$), PMd ($T_7 = 2.522$, $q = 0.0860$), ARC ($T_8 = 1.851$, $q = 0.1646$), PVT ($T_8 = 0.8090$, $q = 0.5744$), MHab ($T_8 = 0.0815$, $q = 0.9749$), lPAG ($T_7 = 2.28$, $q = 0.1135$), dlPAG ($T_7 = 0.9192$, $q = 0.5612$), and dmPAG ($T_7 = 0.0325$, $q = 0.9750$). Each data point represents one animal and for structures that had multiple sections analyzed an average of the animal was taken. For all structures analyzed, n = 4-5 male mice for each group.

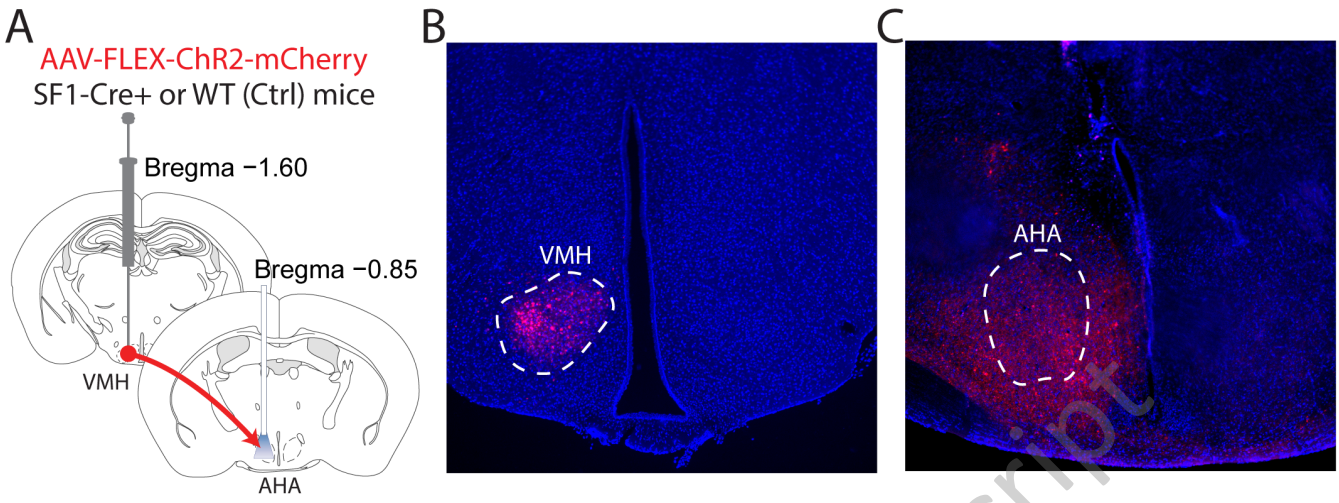
JNeurosci Accepted Manuscript

Figure 8. Physiological and cardiac measures following systemic AMG517 administration. Gray color corresponds to saline-treated mice while red color corresponds to AMG517-treated mice. (A) Body temperature was measured at baseline and 12, 24, and 30 min following systemic saline or AMG517 administration. **(B)** Significantly increased max temperature following AMG517 treatment (Welch's corrected unpaired t-test, $t_{14} = 4.677$, $p = 0.0004$). **(C)** Time course showing significantly increased max temperature following AMG517 treatment. **(D)** No significant difference was detected in heart rate between groups (Welch's corrected unpaired t-test, $t_{12.41} = 1.013$, $p = 0.3302$). **(E)** No significant difference was detected in fractional shortening between groups (Welch's corrected unpaired t-test, $t_{12.99} = 0.5619$, $p = 0.5838$). **(F)** No significant difference was detected in stroke volume between groups (Welch's corrected unpaired t-test, $t_{11.34} = 0.1137$, $p = 0.9114$). **(E)** No significant difference was detected in cardiac output between groups (Welch's corrected unpaired t-test, $t_{9.932} = 0.0051$, $p = 0.9961$). **(G)** No significant difference was detected in M-mode ejection fraction between groups (Welch's corrected unpaired t-test, $t_{12.78} = 0.5669$, $p = 0.5806$). For all temperature n = 8 male mice per group. For echocardiograph data, n = 7-8 male mice per group.

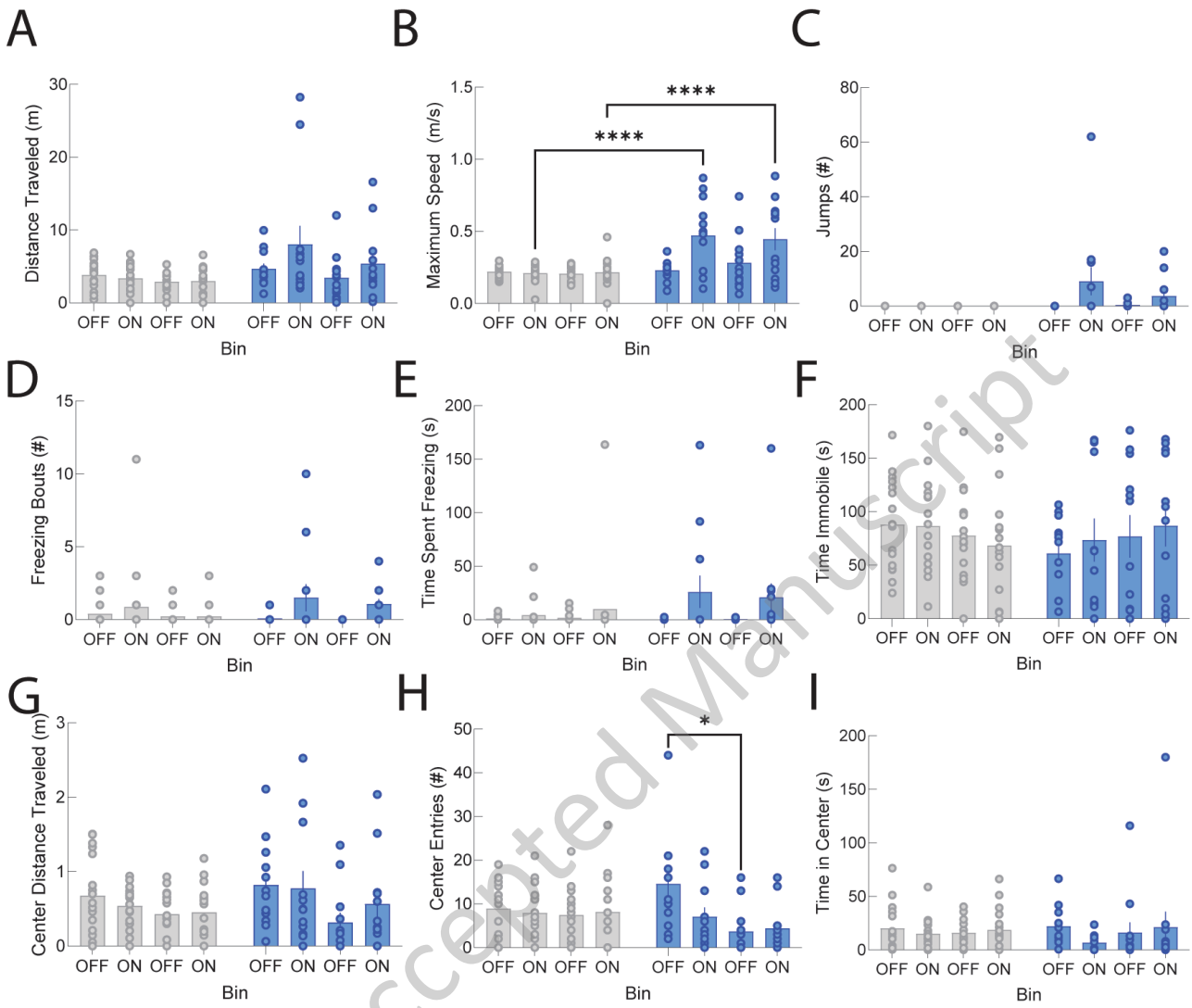
JNeurosci Accepted Manuscript

Figure 9. Open field behavior following systemic AMG517 administration. Gray color corresponds to saline-treated mice while red color corresponds to AMG517-treated mice. **(A)** No significant difference was detected in total distance traveled between groups (Welch's corrected unpaired t-test, $t_{13.01} = 1.194$, $p = 0.2539$). **(B)** No significant difference was detected in maximum speed between groups (Welch's corrected unpaired t-test, $t_{13.50} = 1.541$, $p = 0.1465$). **(C)** No significant difference was detected in jumping behavior between groups (Welch's corrected unpaired t-test, $t_{7.000} = 1.000$, $p = 0.3506$). **(D)** No significant difference was detected in freezing bout number between groups (Welch's corrected unpaired t-test, $t_{7.465} = 2.100$, $p = 0.0715$). **(E)** No significant difference was detected in time spent freezing between groups (Welch's corrected unpaired t-test, $t_{7.272} = 2.038$, $p = 0.0795$). **(F)** No significant difference was detected in time immobile between groups (Welch's corrected unpaired t-test, $t_{11.31} = 1.164$, $p = 0.2685$). **(G)** No significant difference was detected in center distance between groups (Welch's corrected unpaired t-test, $t_{8.944} = 0.3423$, $p = 0.7400$). **(H)** No significant difference was detected in center entries between groups (Welch's corrected unpaired t-test, $t_{12.85} = 0.4971$, $p = 0.6275$). **(I)** No significant difference was detected in time in center between groups (Welch's corrected unpaired t-test, $t_{13.53} = 0.8069$, $p = 0.4337$). **(J)** No significant difference was detected in latency to escape between treatment groups (Welch's corrected unpaired t-test, $t_{7.000} = 1.000$, $p = 0.3506$). **(K)** Escape success rate was not significantly different between saline- and AMG517-treated mice (Fisher's exact test, $p > 0.9999$). **(L)** No significant difference was detected in time spent in the open arms between groups (Welch's corrected unpaired t-test, $t_{10.36} = 0.7745$, $p = 0.4560$). **(M)** No significant difference was detected in open arm entries between groups (Welch's corrected unpaired t-test, $t_{13.40} = 0.6036$, $p = 0.5562$). **(N)** No significant difference was detected in open arm distance between groups (Welch's corrected unpaired t-test, $t_{13.38} = 0.4620$, $p = 0.6515$). **(D)** No significant difference was detected in time spent in the closed arms between groups (Welch's corrected unpaired t-test, $t_{13.15} = 0.03386$, $p = 0.9735$). **(O)** No significant difference was detected in closed arm entries between groups (Welch's corrected unpaired t-test, $t_{12.10} = 1.117$, $p = 0.2855$). **(P)** No significant difference was detected in closed arm distance between groups (Welch's corrected unpaired t-test, $t_{8.878} = 1.448$, $p = 0.1823$). **(Q)** No significant difference was detected in total distance traveled between groups (Welch's corrected unpaired t-test, $t_{10.28} = 1.144$, $p = 0.2786$). **(R)** No significant difference was detected in center entries between groups (Welch's corrected unpaired t-test, $t_{13.73} = 0.7741$, $p = 0.4520$). **(S)** No significant difference was detected in head dip entries between groups (Welch's corrected unpaired t-test, $t_{12.82} = 0.1896$, $p = 0.8526$). For all behavior data, n = 7-8 male mice per group.

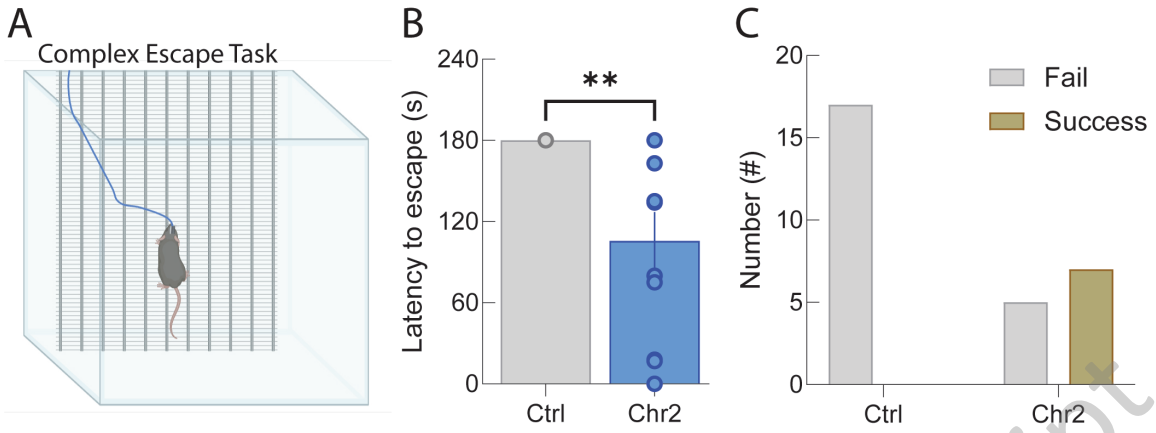
JNeurosci Accepted Manuscript



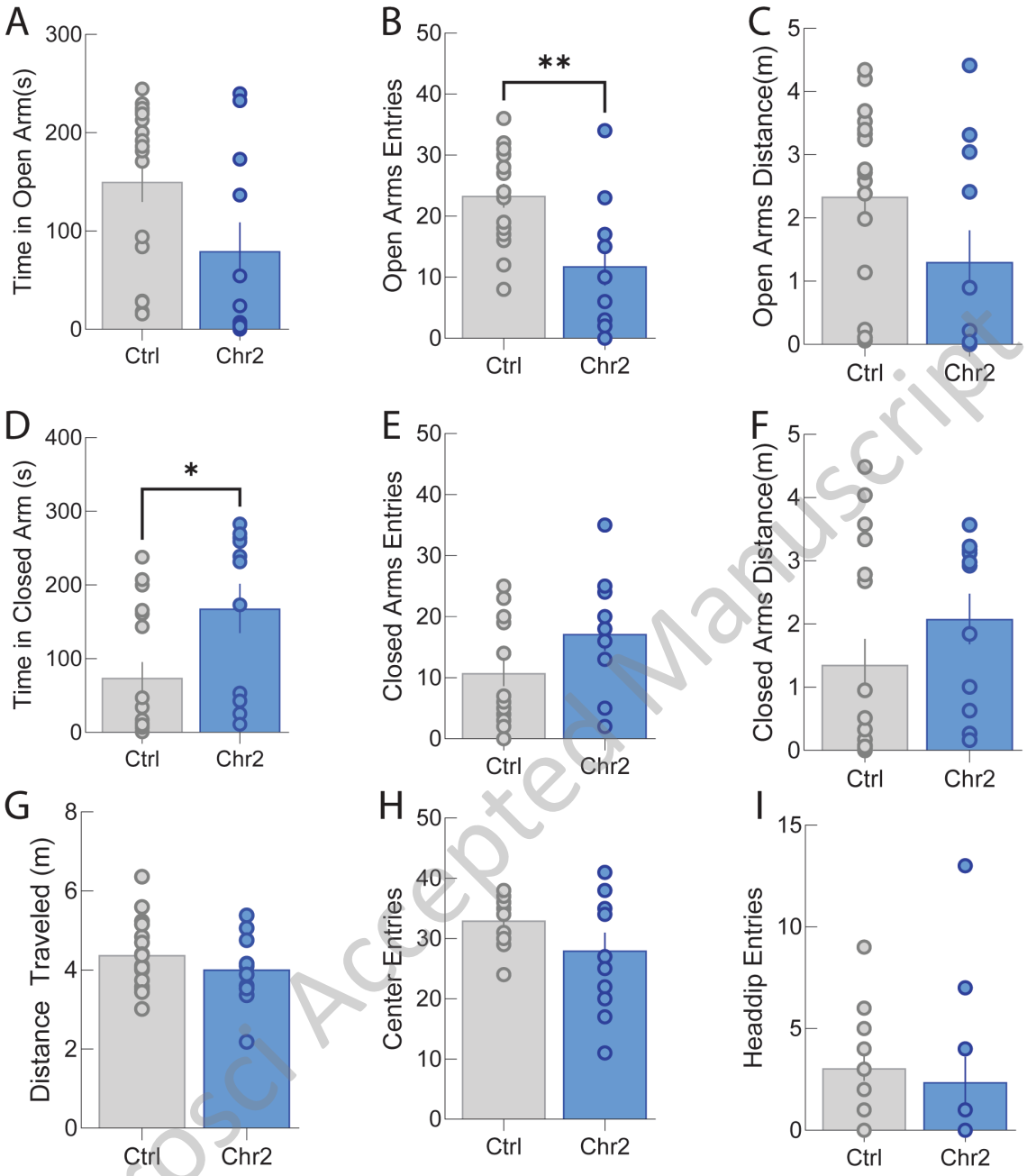
JNeurosci Accepted Manuscript



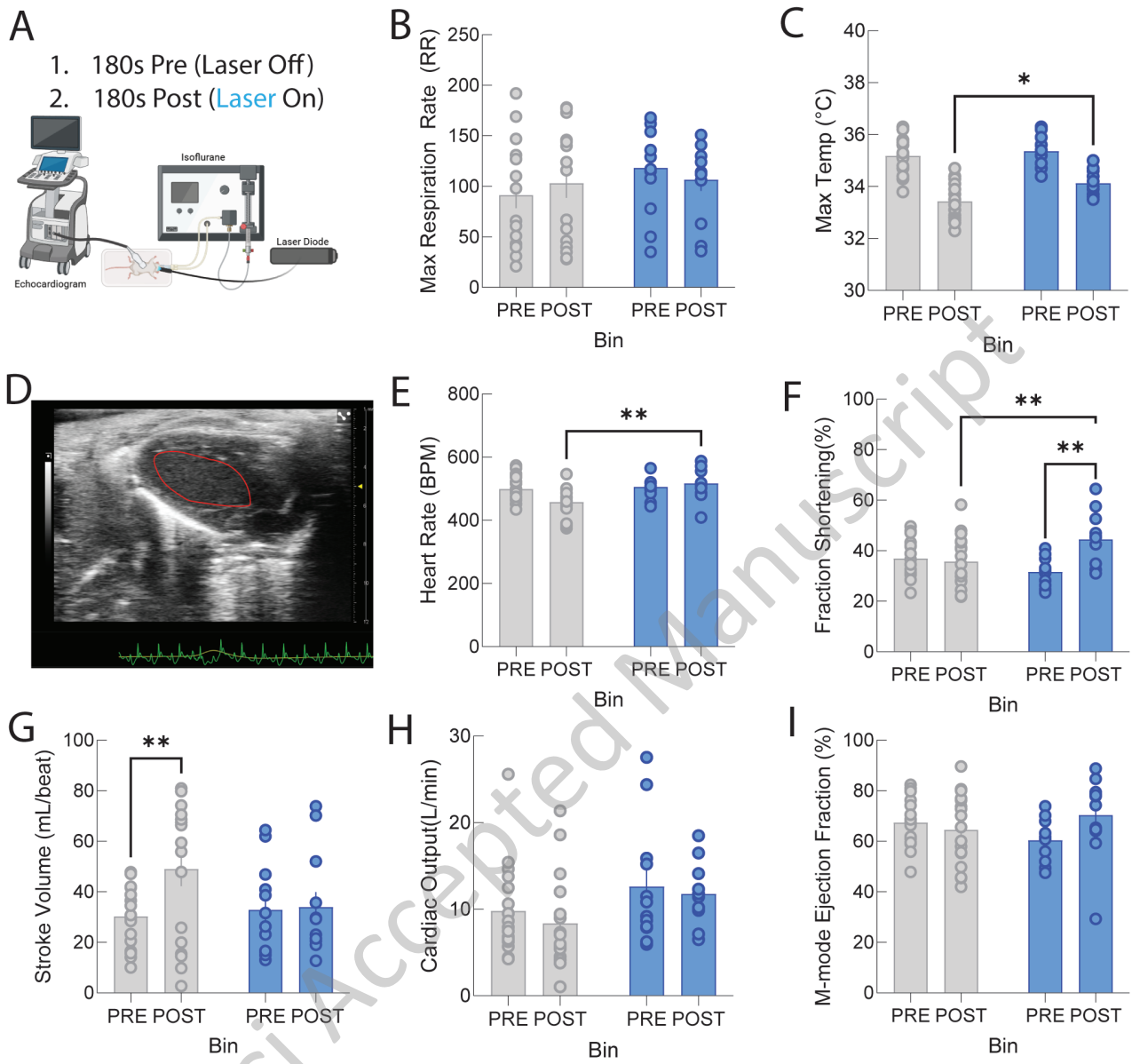
JNeurosci Accepted Manuscript



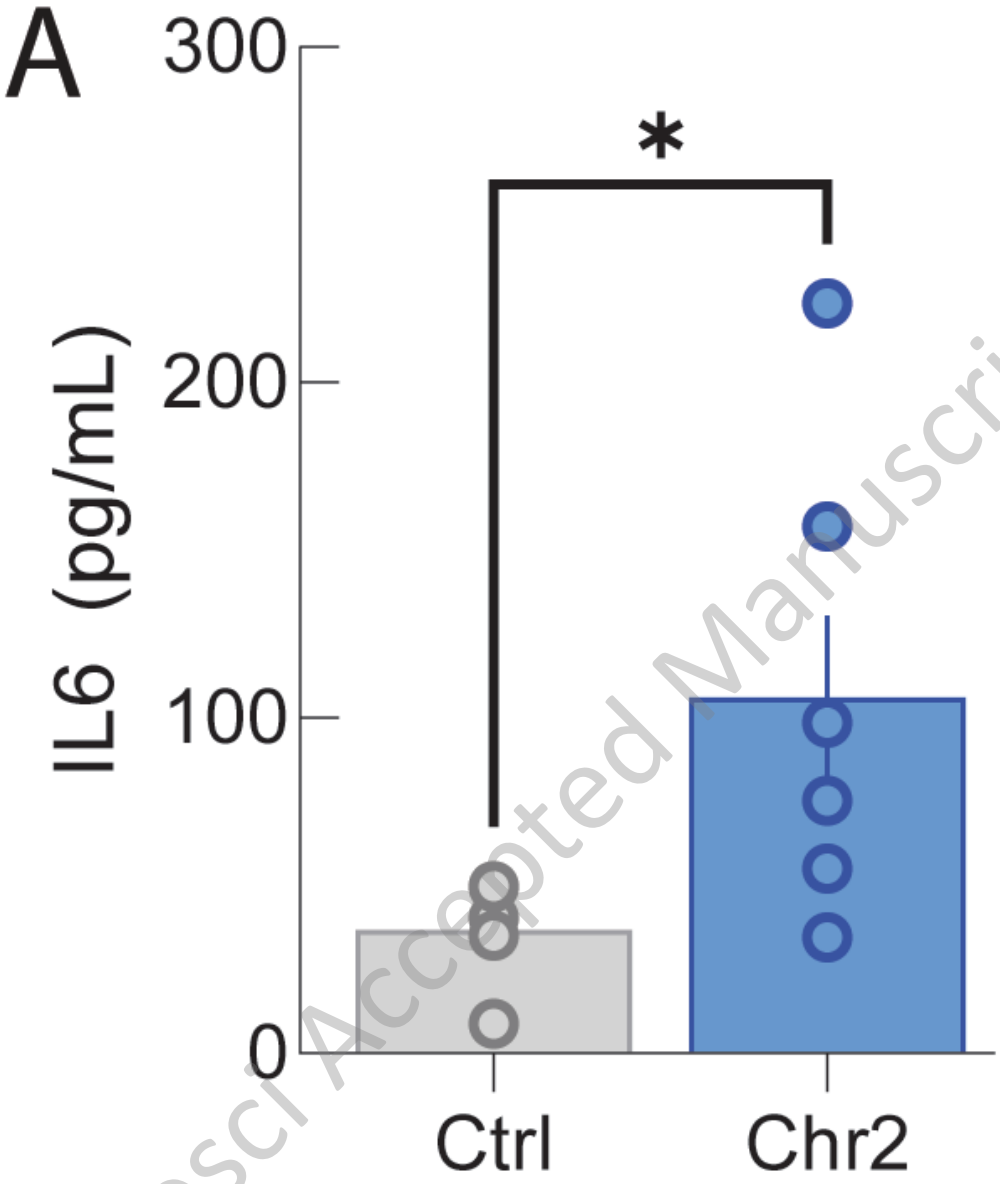
JNeurosci Accepted Manuscript



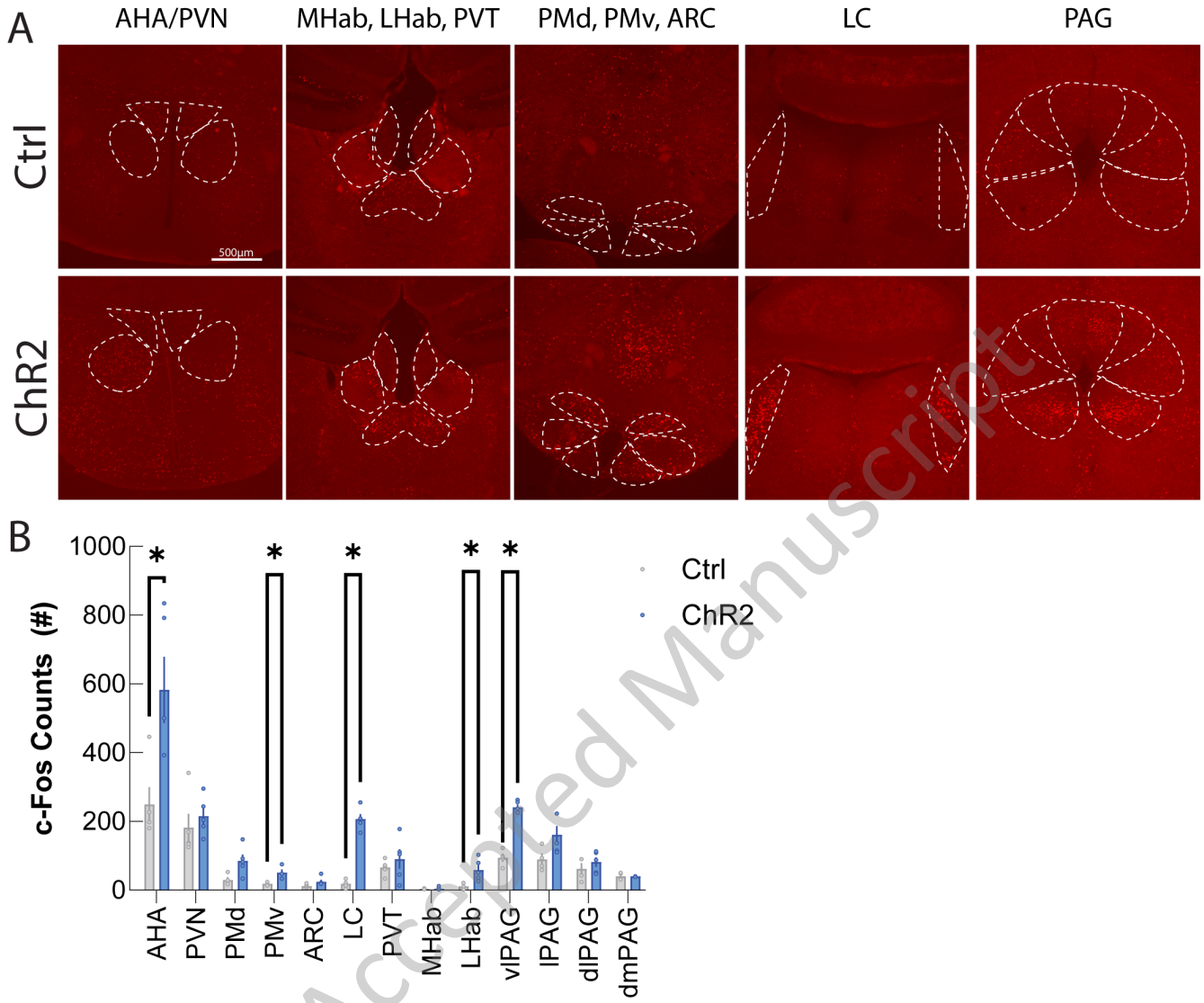
JNeuroSci Accepted Manuscript



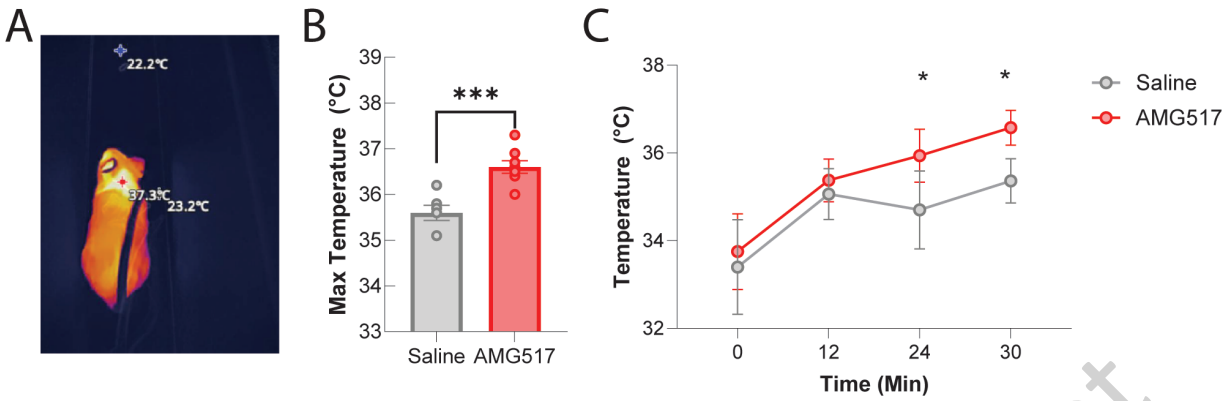
JNeurosci Accepted Manuscript



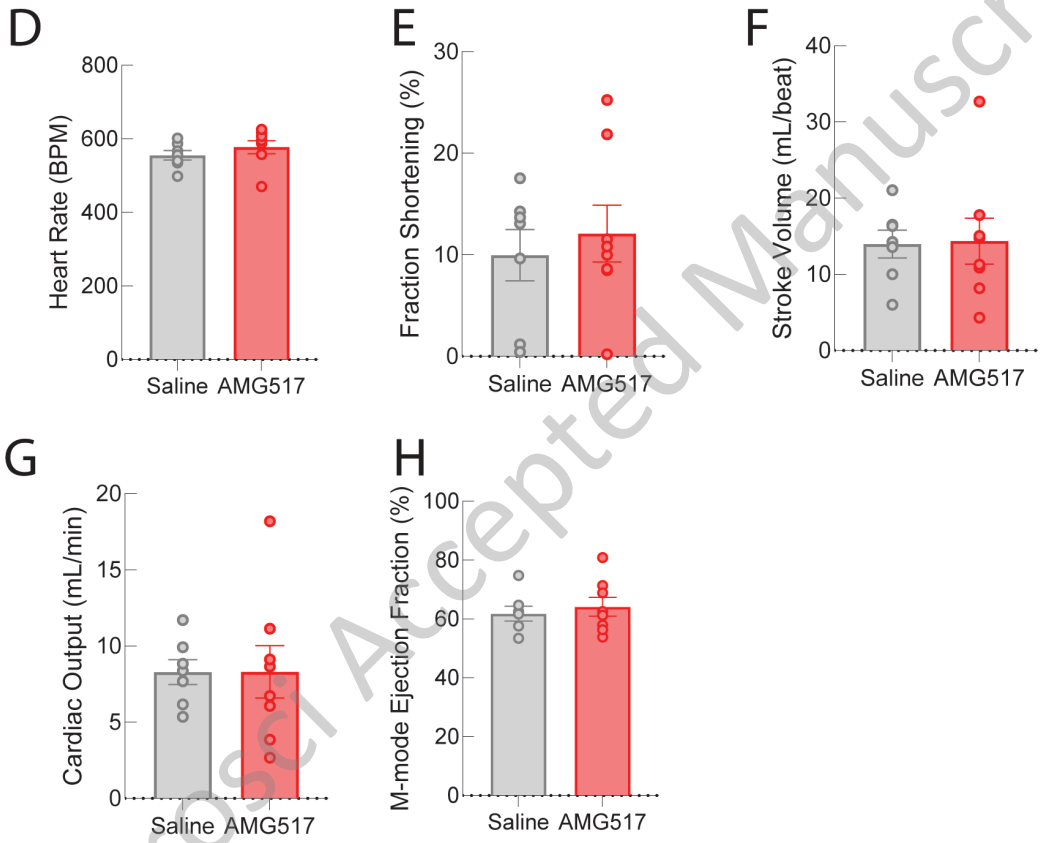
JNeurosci Accepted Manuscript



JNeurosci Accepted Manuscript

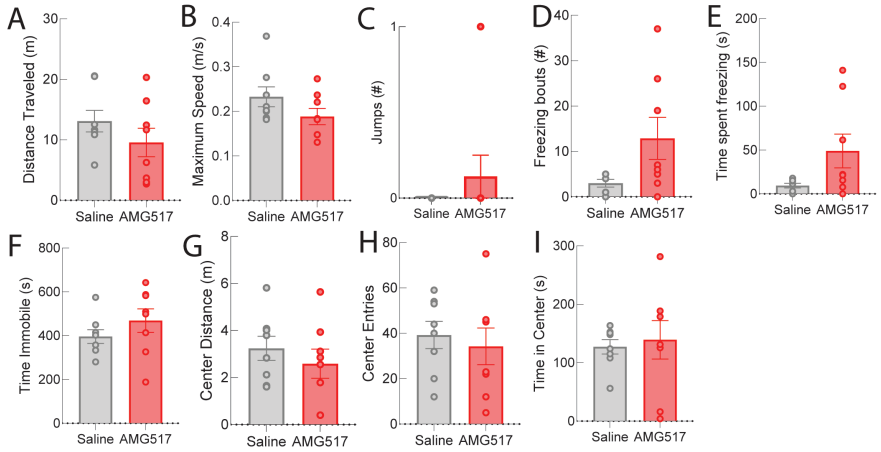


Echocardiogram

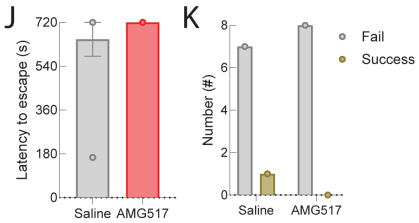


JNeurosci Accepted Manuscript

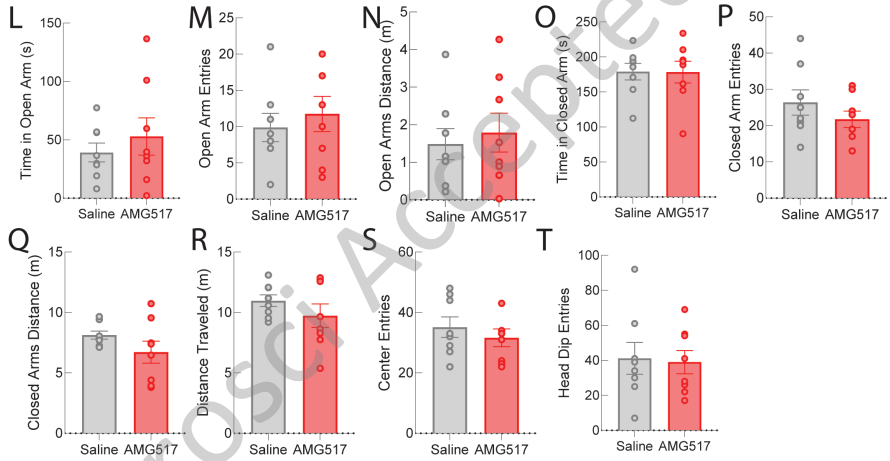
Open Field Test



Complex Escape



Elevated Plus Maze



JNeurosci Accepted Manuscript